Hindawi
International Journal of Antennas and Propagation
Volume 2018, Article ID 3563949, 10 pages
https://doi.org/10.1155/2018/3563949

Research Article

A Compact Dual-Band Circularly Polarized Antenna with Wide HPBWs for CNSS Applications

Chao Li, Fu-Shun Zhang, Fan Zhang, and Kaiwen Yang

National Laboratory of Antennas and Microwave Technology, Xidian University, Xi'an, Shaanxi 710071, China

Correspondence should be addressed to Chao Li; lichao972@126.com

Received 9 November 2017; Revised 22 December 2017; Accepted 26 December 2017; Published 4 March 2018

Academic Editor: Ikmo Park

A compact dual-band circularly polarized antenna with wide half-power beamwidths (HPBWs) for compass navigation satellite system applications is proposed in this paper. The CP radiation is realized by arranging four compact dual-band inverted-F monopoles symmetrically to the center point, where the four monopoles are excited with a 90° phase offset through a compact sequential-phase feeding network. The compactness of the dual-band inverted-F monopole is realized by inserting two chip inductors in the horizontal portion of the monopole. The overall dimension of the antenna is only $0.211\lambda_0 \times 0.211\lambda_0 \times 0.057\lambda_0$, where λ_0 is the corresponding free-space wavelength at 1.268 GHz. Experimental results show that the proposed antenna exhibits two overlapped impedance and axial ratio bandwidths of 50 MHz (1.236–1.286 GHz) and 40 MHz (1.532–1.572 GHz). Wide HPBWs of about 120°/125° and 121°/116° (XOZ/YOZ planes) at center frequencies (1.268, 1.561 GHz) of the CNSS-2 B3 and B1 bands are obtained, respectively. With these good performances, the antenna can be a good candidate for CNSS applications.

1. Introduction

In recent years, satellite navigation systems have been widely used in human life for civilian and military applications. Among them all, the compass navigation satellite system (CNSS) has attracted more and more attentions due to the navigation and positioning services compatible with other systems. In some applications of the CNSS-2, terminals are required to operate at B3 (1.268 GHz ± 10 MHz) and B1 (1.561 GHz ± 2 MHz) bands with a right-hand circular polarization (RHCP) radiation pattern. Nevertheless, with the dimensions of the CNSS terminals getting smaller, a compact dual-band CP antenna covering both the bands is highly demanded.

Many dual-band circularly polarized (CP) antennas with compact dimensions have been reported, and they can be divided into three types in summary. The microstrip antenna is the most common type used for dual-band GNSS applications. Various kinds of techniques are used to reduce the antenna dimension, such as adopting high-permittivity substrates in [1–3], grounding the central patches surrounded by four square-ring-shaped slots ($0.396\lambda_0 \times 0.396\lambda_0 \times 0.048\lambda_0$) in [4], loading two shorting probes in parallel ($0.23\lambda_0 \times 0.23\lambda_0 \times 0.07\lambda_0$) in [5], utilizing the structure of a split patch surrounded by a split ring ($0.289\lambda_0 \times 0.289\lambda_0 \times 0.099\lambda_0$) in [6], and using truncated corner square patch radiators stacked over a reactive impedance surface to reduce the electrical size of the antenna for lower band in [7, 8]. The ring-shaped patch antenna is another way to achieve a compact size. In [9, 10], the fundamental modes of the ring resonators are excited by employing meandering slots and integrating a locally grounded coupler, respectively, to reduce their dimensions. Concentric annular rings ($0.259\lambda_0 \times 0.259\lambda_0 \times 0.048\lambda_0$) in [11], rectangular rings ($0.231\lambda_0 \times 0.231\lambda_0 \times 0.084\lambda_0$) in [12], and meandered-line-shaped rings ($0.201\lambda_0 \times 0.201\lambda_0 \times 0.076\lambda_0$) in [13] are printed on the same layer or different layers, respectively, to obtain reduced antenna dimensions. Apart from the two types mentioned above, various kinds of compact dual-band CP crossed-dipole antennas have been reported. In [14], asymmetrically barbed arrowheads and printed inductors are inserted in each dipole arm to reduce the antenna dimension. In [15, 16], complementary split-ring resonators and four-arm curl of different arm lengths are used to achieve

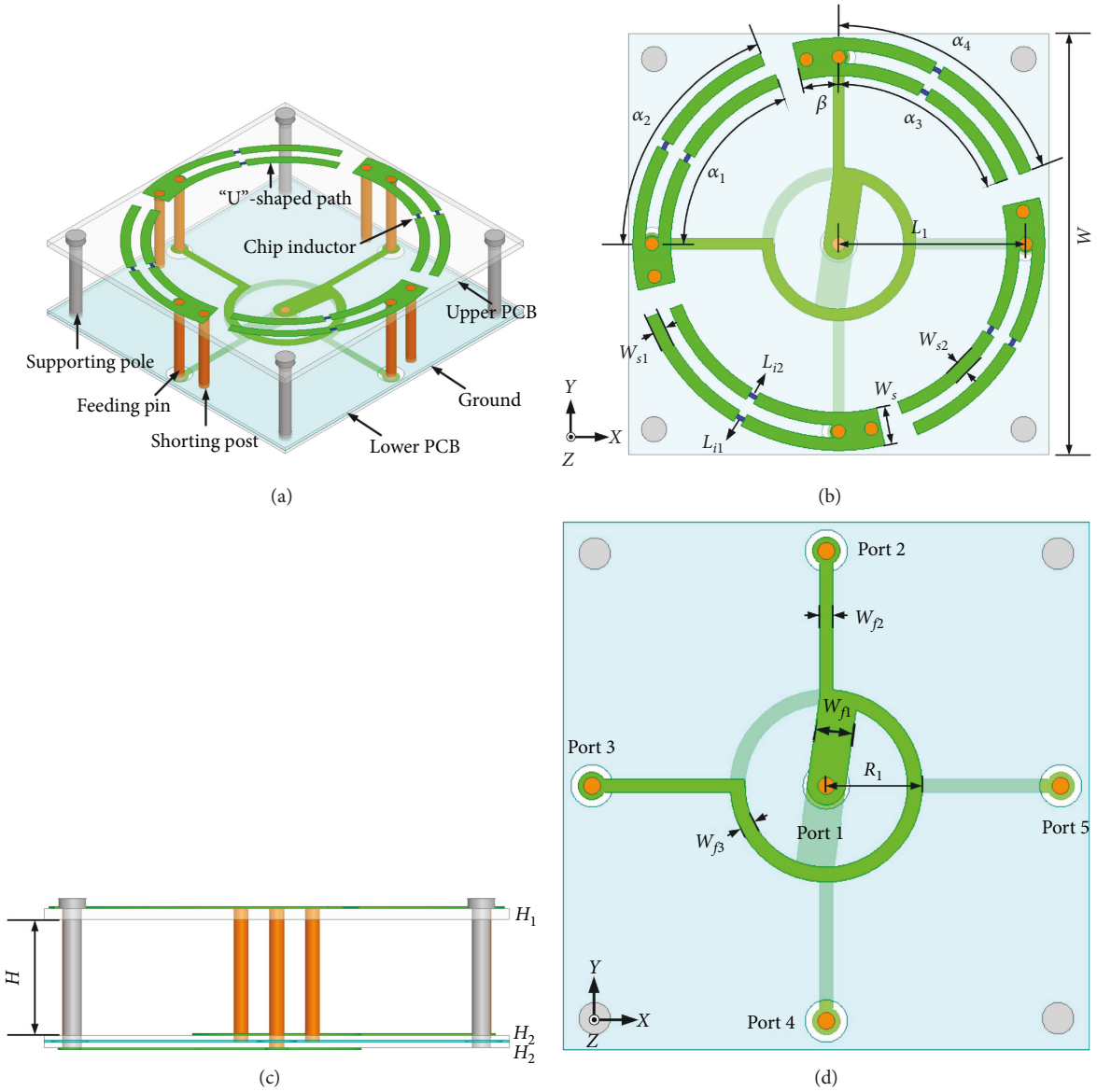

FIGURE 1: Geometry of the proposed antenna: (a) 3D view; (b) top view; (c) side view; (d) feeding network.

dual-band operations and compact dimensions. However, the profiles of these crossed-dipole antennas are relatively high due to the generally needed metal cavities in them. Although the dimensions of the antennas are reduced by these techniques, they may suffer from complicated structures and narrow radiation patterns with HPBWs of less than 100° in general.

Wide half-power beamwidths (HPBWs) are very valuable in CNSS applications in order to improve the coverage area and stabilize the receiving signal. Many studies have been done to broaden the HPBWs of the antenna, such as extending the substrate beyond the ground plane with HPBWs of 130° in [17], loading auxiliary radiators with HPBWs of 90° in [18], loading with curved microstrip resonant structure with HPBWs of 150° in [19], utilizing the curved dipoles and ground planes with HPBWs of 150° in [20], and adopting various kinds of conducting wall or cavity with HPBWs of greater than 100° in [21–24] which is the most common way. Nevertheless, the antennas mentioned above have relatively large dimensions, and most of them focus on single-band work.

In this paper, a compact dual-band CP antenna with wide HPBWs is proposed. Four compact inverted-F monopoles are arranged symmetrically to the center point and fed by a compact sequential-phase (SP) feeding network to get the CP radiation. With the use of the shorting technique and chip inductors, the compactness of the dual-band inverted-F monopole is obtained. The overall dimension of the antenna is only $0.211\lambda_0 \times 0.211\lambda_0 \times 0.057\lambda_0$, where λ_0 is the corresponding free-space wavelength at 1.268 GHz. The two impedance bands ($|S_{11}| < -10$ dB) are 72 MHz (1.236–1.308 GHz) and 96 MHz (1.52–1.616 GHz), while

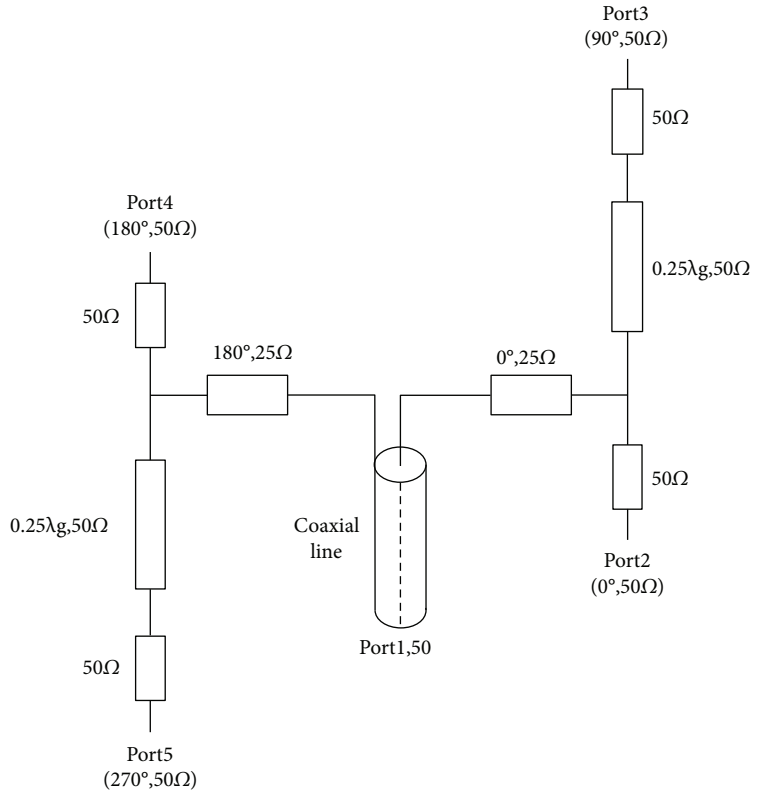

Figure 2: Equivalent-circuit model of the feeding network.

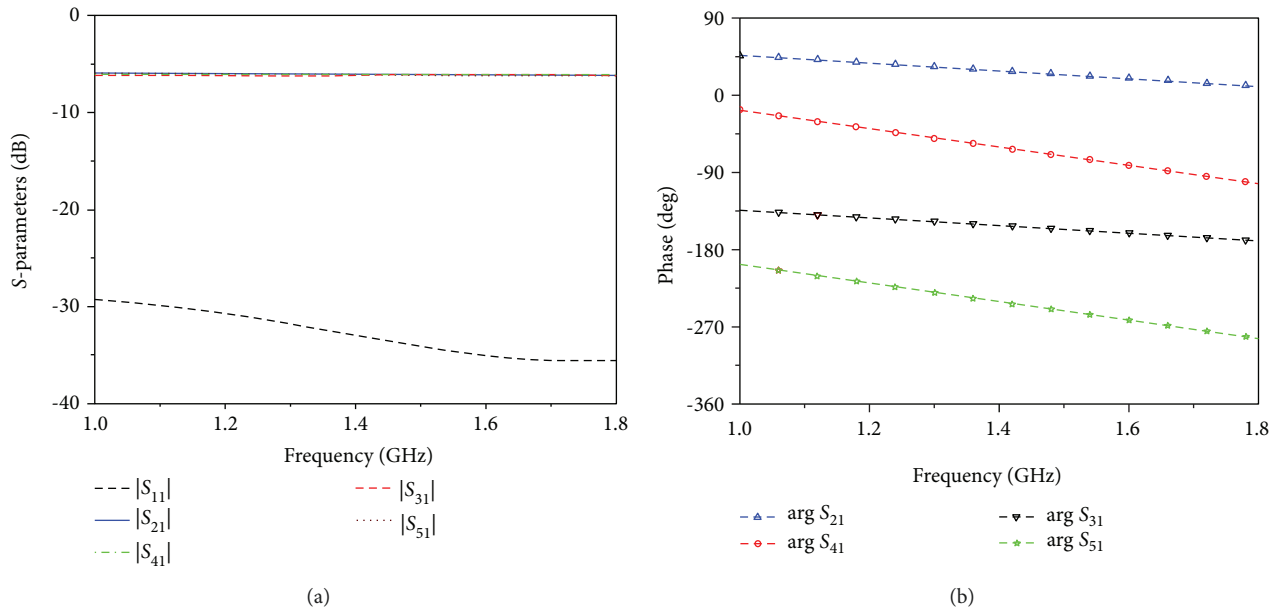

Figure 3: Simulated (a) *S*-parameters and (b) transmission phases of the SP feeding network.

the corresponding axial ratio (AR) bands (AR < 3 dB) are 54 MHz (1.232–1.286 GHz) and 40 MHz (1.532–1.572 GHz), covering the CNSS-2 B3 and B1 bands, respectively. Meanwhile, the HPBWs at 1.268 GHz and 1.561 GHz are both greater than 115°. Details of the proposed antenna design are presented in Section 2.

2. Antenna Geometry and Design Process

2.1. Antenna Geometry. The geometry of the proposed antenna is shown in Figure 1. The antenna is composed of three parts: the upper printed circuit board (PCB), the lower PCBs (including two substrates), and the middle connecting

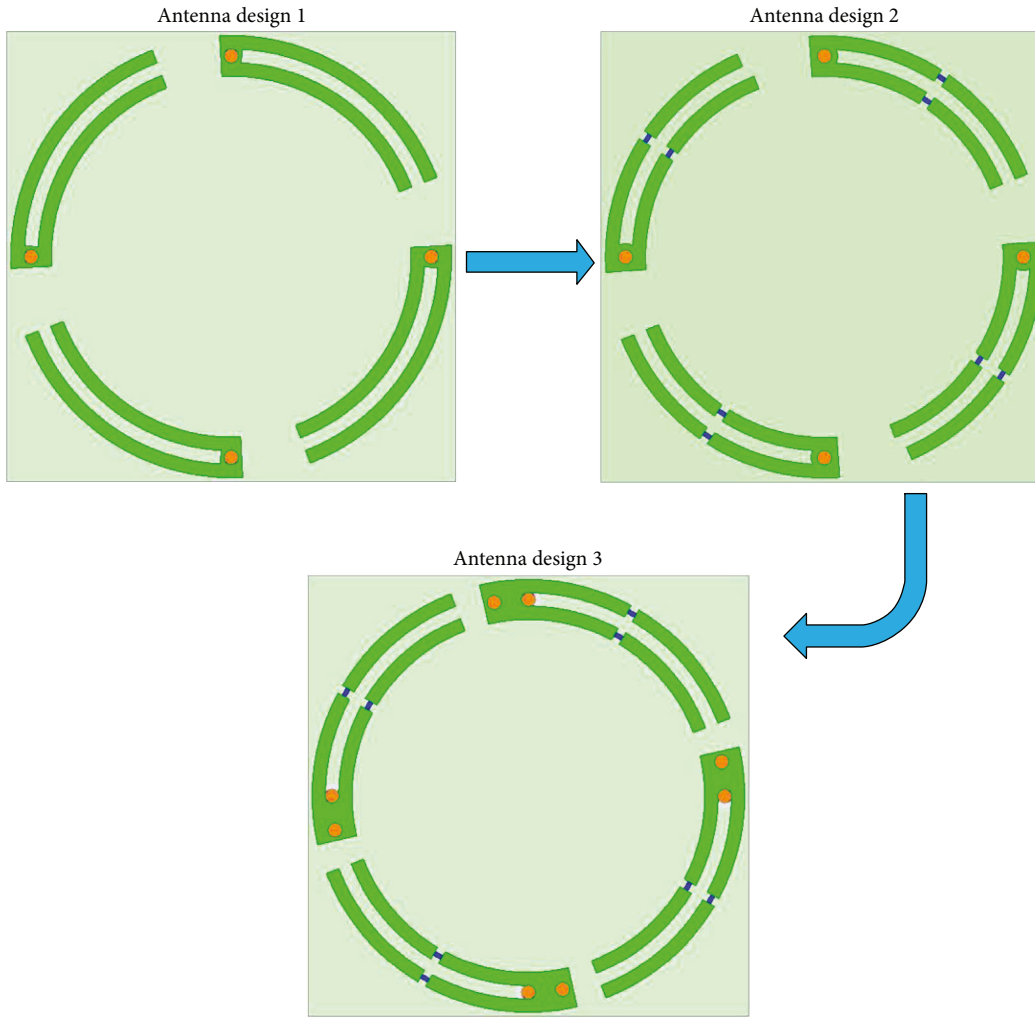

Figure 4: The design process of the proposed antenna.

structures (including feeding pins, metallic shorting posts, and nonmetallic supporting poles).

The upper PCB is a 1 mm thick FR4 substrate with a relative permittivity of 4.4. Four "U"-shaped patches (with radius of L_1) composed of two connected arc-shaped arms are etched on the top layer of the upper substrate. The two arc-shaped arms with different radius and angles are resonant at different frequencies. Two chip inductors with different inductance (L_{i1} and L_{i2}) are inserted in the two arms of the "U"-shaped patch, respectively. Each upper patch is connected to the feeding network by a feeding pin (with a radius of 0.8 mm) and is shorted to the metal ground by a metallic shorting post (with a radius of 0.8 mm) at the initial portion (with angle β). Thus, the "U"-shaped patch can be regarded as a dual-band inverted-F monopole. The inverted-F monopoles are arranged symmetrically to the center point of the antenna and excited with 90° phase offsets through a compact SP feeding network. Four nonmetallic poles are employed as the structural support between the upper and lower PCBs.

The lower PCBs are composed of two substrates, and both of them are 0.5 mm thick PTFE substrates with a relative permittivity of 2.65. The SP feeding network is composed of

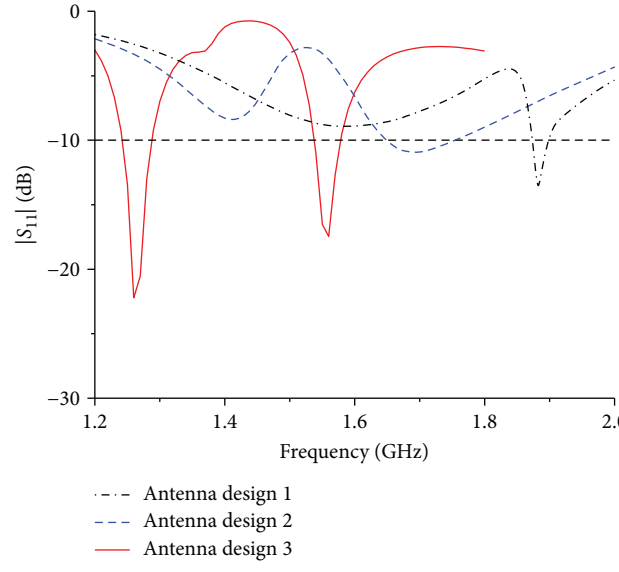

Figure 5: The simulated $|S_{11}|$ of the three antenna designs.

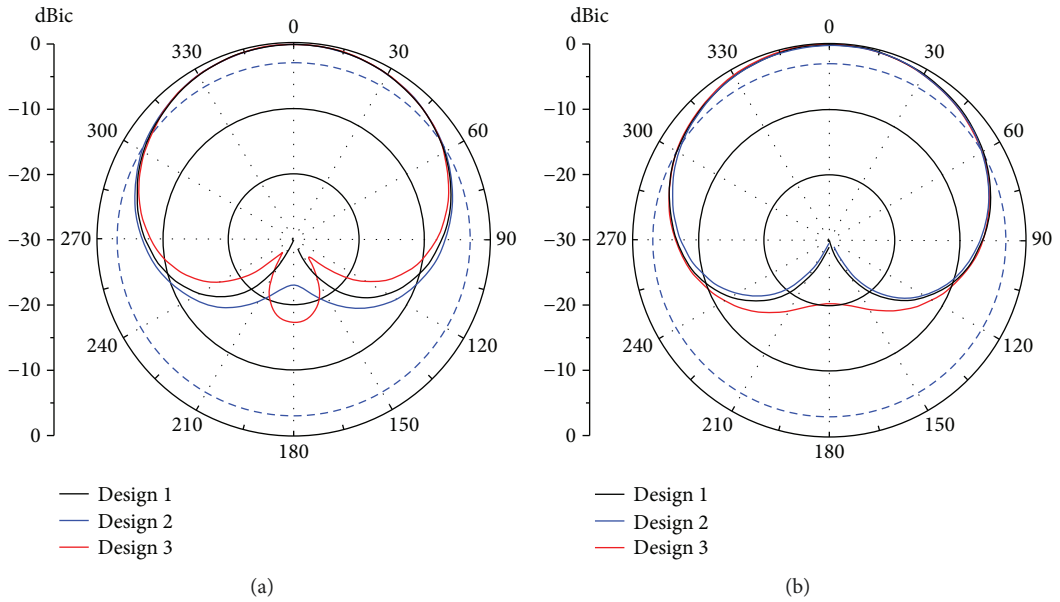

Figure 6: Normalized radiation patterns of the three designs at (a) low band and (b) high band.

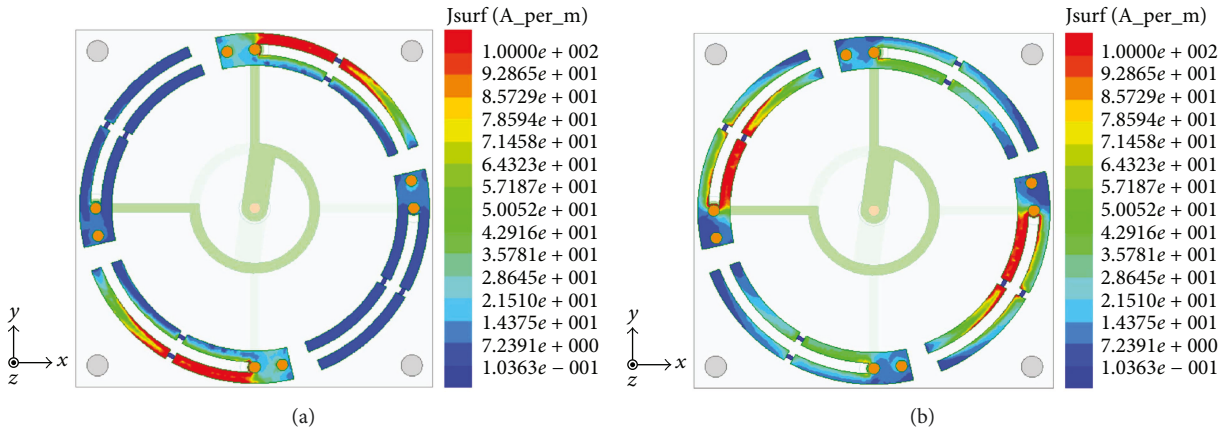

Figure 7: Simulated current distributions of the proposed antenna at (a) 1.268 GHz and (b) 1.561 GHz.

three layers on the two substrates. Figure 1(d) shows the layout of the feeding lines of the SP feeding network. A 50 Ω coaxial line is used as the input feeding structure, and the middle layer is used as the ground plane. The outer conductor of the coaxial line is connected to the bottom layer, whereas the inner conductor is connected to the top layer. A circular aperture at the center point is removed from the ground plane on the middle layer. Unlike the feeding network in [25], the microstrip transmission lines are positioned on the opposite sides of the ground plane rather than on the same side. Two concentric vacant-quarter rings are etched on the top and bottom layers, respectively, with the same outer radius R_f and microstrip transmission line widths (W_{f1}, W_{f2}, and W_{f3}).

The equivalent-circuit model of the SP feeding network is shown in Figure 2. Based on the out-of-phase property between the inner and outer conductors of the coaxial line, a stable 180° phase difference between the top and bottom layers is achieved. In order to achieve impedance matching,

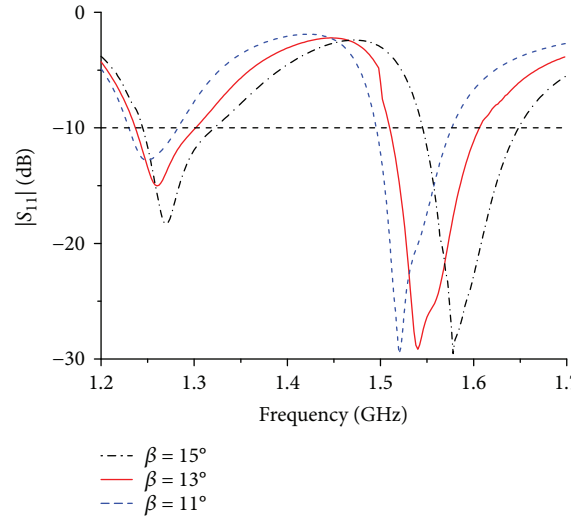

Figure 8: Simulated $|S_{11}|$ for various values of β.

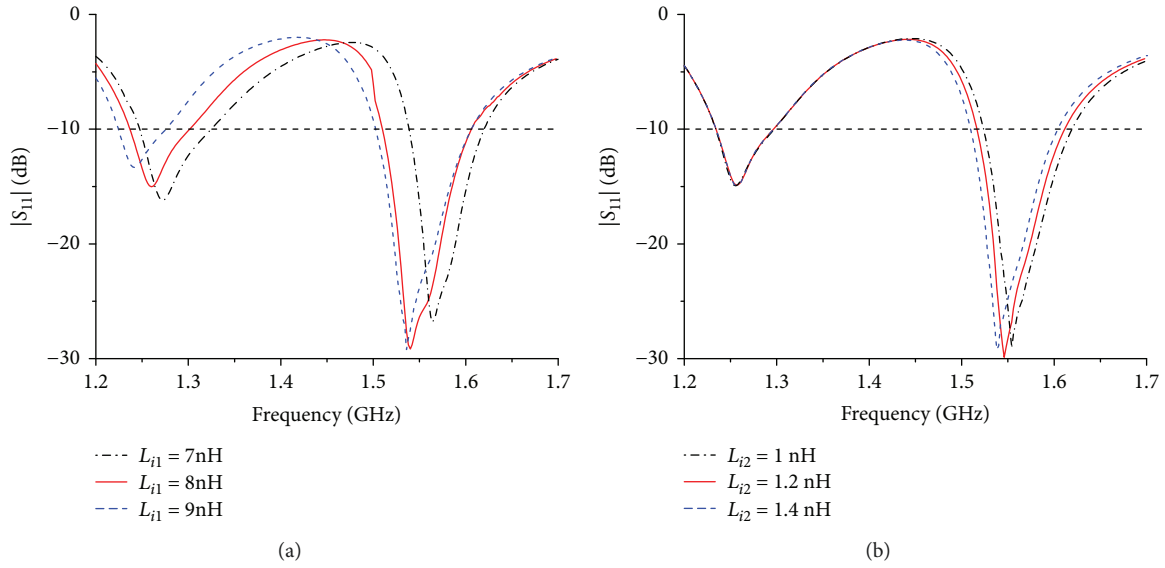

Figure 9: Simulated $|S_{11}|$ for various values of (a) L_{i1} and (b) L_{i2}.

Figure 10: Prototype of the proposed antenna: (a) top view; (b) side view.

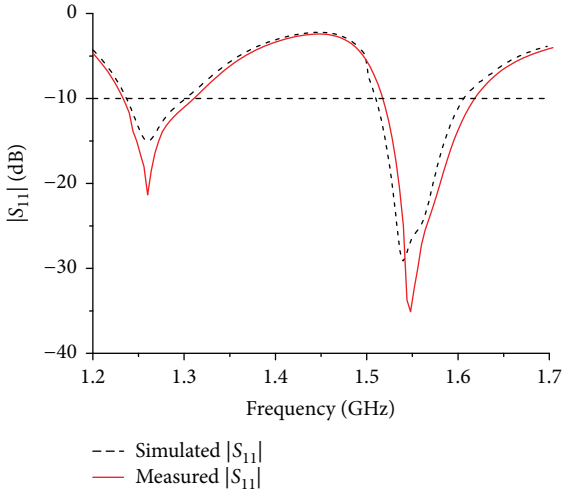

Figure 11: Simulated and measured $|S_{11}|$ of the proposed antenna.

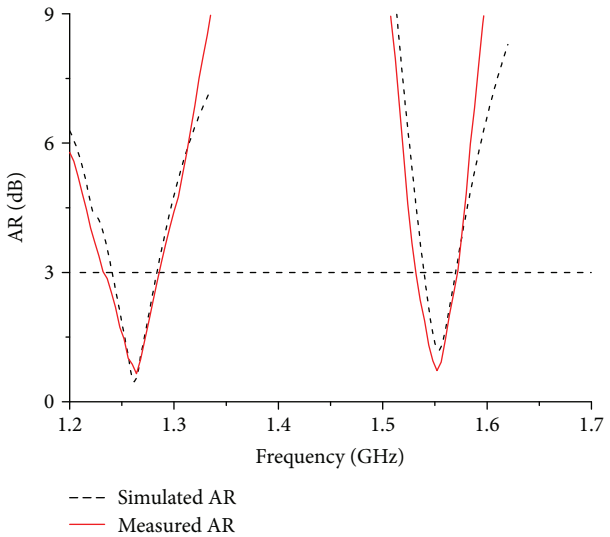

Figure 12: Simulated and measured AR of the proposed antenna.

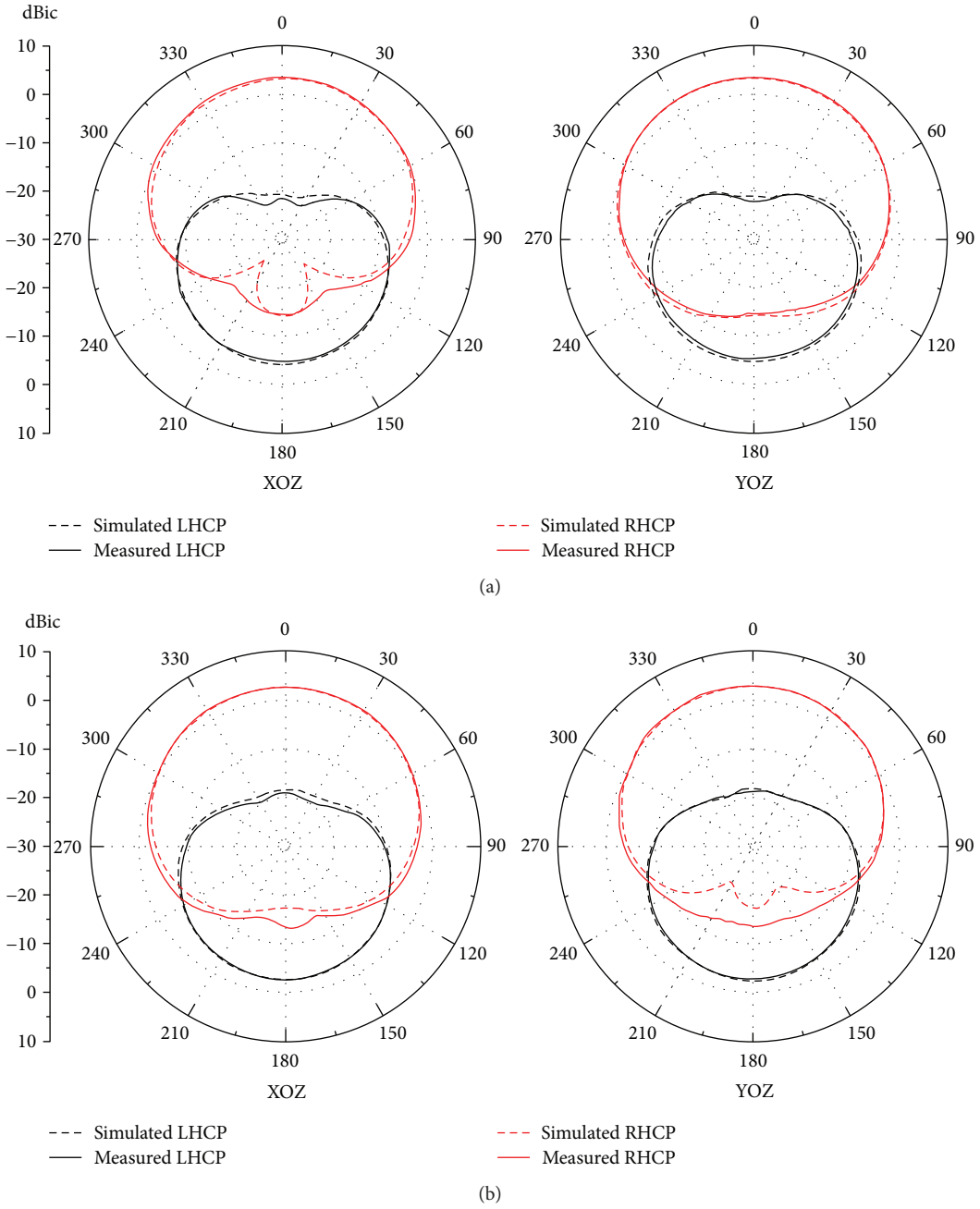

Figure 13: Simulated and measured radiation patterns at (a) 1.268 GHz and (b) 1.561 GHz.

the characteristic impedance of the microstrip transmission line with width W_{f1} near the feeding point is chosen as 25 Ω, while that of the lines with widths W_{f1} and W_{f2} is chosen as 50 Ω. The two concentric vacant-quarter rings are used as 90° phase delay lines to achieve 90° phase offsets between the four output ports.

Figure 3 shows the simulated S-parameters and transmission phases of the SP feeding network. As shown in Figure 3(a), the transmission coefficients (from $|S_{21}|$ to $|S_{51}|$) are -6.1 ± 0.3 dB, while the reflection coefficients at port 1 ($|S_{11}|$) is below −29 dB across the frequency range of 1.0–1.8 GHz. As shown in Figure 3(b), a phase difference of approximately $90° \pm 5°$ is achieved between the adjacent output ports in the frequency range of 1.2–1.7 GHz.

The phase differences caused by the vacant-quarter rings are different at high and low bands. In order to compensate the phase difference between the two operating bands, the arc-shaped arm's lengths of the adjacent inverted-F monopoles are slightly different ($\alpha_1 \neq \alpha_3$, $\alpha_2 \neq \alpha_4$), whereas the opposite monopoles are of the same dimension. The optimized antenna design parameters are as follows: $W = 50$ mm, $W_s = 4.5$ mm, $W_{s1} = W_{s2} = 1.5$ mm, $W_{f1} = 3.6$ mm, $W_{f2} = 1.2$ mm, $W_{f3} = 1.4$ mm, $R_f = 9.1$ mm, $L_1 = 22.2$ mm, $L_{i1} = 8.2$ nH, $L_{i2} = 1.2$ nH, $\alpha_1 = 69.5°$, $\alpha_2 = 67.5°$, $\alpha_3 = \alpha_4 = 69°$, $\beta = 13°$, $H = 11.5$ mm, $H_1 = 1$ mm, and $H_2 = 0.5$ mm.

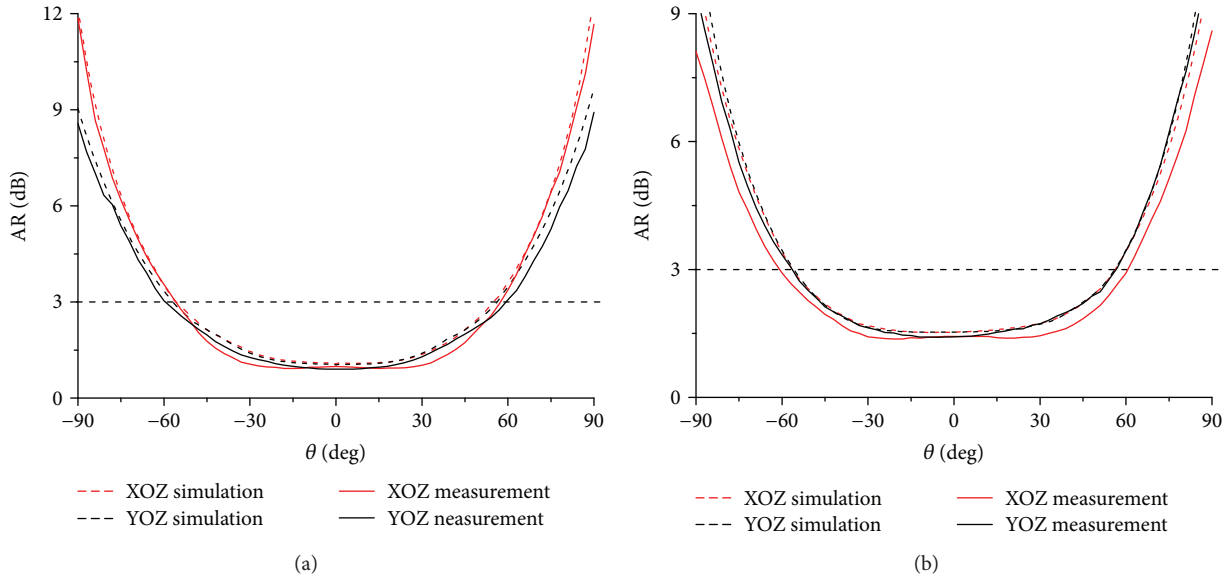

Figure 14: Simulated and measured AR at (a) 1.268 GHz and (b) 1.561 GHz.

2.2. Antenna Design Process. Figure 4 shows the design process of the proposed antenna. The initial design (design 1) can be regarded as four "U"-shaped monopoles symmetrically arranged to the center point. Then two chip inductors with inductance L_{i1} and L_{i2} are inserted in both arms of the monopole antenna (design 2). Finally, the shorting load technique is used to achieve size reduction. An arc-shaped arm of angle β and width W_s is added to the connected portion of the "U"-shaped monopole and shorted to the ground by a metallic shorting post. After adopting the shorting load technique, the "U"-shaped monopole is transformed into an inverted-F monopole antenna (design 3). All of the three designs use the same FR4 and PTFE substrates with the same dimension of $50 \times 50 \times 13.5\,\text{mm}^3$.

The simulated $|S_{11}|$ of the three designs without the feeding network is shown in Figure 5. As can been seen from Figure 4, from design 1 to design 2, the resonant frequency shifts downwards. The main reason is that effective electric lengths of the arms are increased due to the inserted inductors. From design 2 to design 3, the resonant frequency decreases further because of the coupling capacitance between the shorting post and the antenna. It indicates that by using the shorting loaded technique and inserting chip inductors, the compactness of the antenna can be obtained.

Figure 6 shows the normalized RHCP radiation patterns of the three designs at the corresponding resonant frequencies of the low and high bands in the XOZ plane, respectively. As can be seen in Figure 6, all of the three designs have wide HPBWs greater than 110°. This phenomenon occurs mainly due to the vertical currents of the feeding pins and shorting posts and the relative shorter distance between the four monopoles.

Figure 7 shows the simulated current distributions of the proposed antenna at 1.268 GHz and 1.561 GHz. It is obvious that at the low band, the current mainly focuses on the outer arc-shaped arm of the inverted-F monopole, whereas there is little current distributed on the inner one, while at the high band, the current mainly focuses on the inner one.

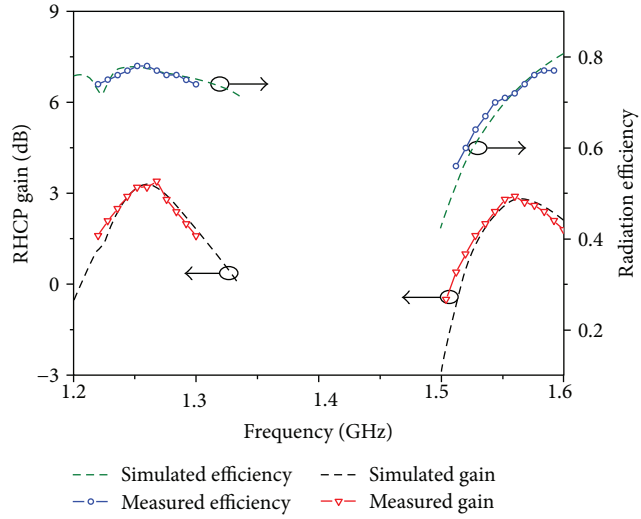

Figure 15: Simulated and measured boresight RHCP gains and radiation efficiencies.

3. Parametric Study

According to the antenna design process, the shorting loaded technique and inserted chip inductors are the main ways to reduce the antenna dimension; thus, the angle β of the shorting arc-shaped arm and the inductance (L_{i1} and L_{i2}) of the two chip inductors have been studied.

Figure 8 shows the simulated $|S_{11}|$ with different values of angle β. As shown in Figure 8, with β varying from 15° to 11°, the resonant frequencies at the low and high bands both decrease. It means that decreasing the length of the shorting arc-shaped arm can enhance the coupling capacitance between the shorting post and the antenna, which can reduce the antenna dimension.

The simulated $|S_{11}|$ with different values of L_{i1} and L_{i2} is shown in Figures 9(a) and 9(b), respectively. It can be seen

Table 1: Performance comparison between the proposed antenna and the previous dual-band antennas.

Antenna structure	Overall dimension	−10 dB $\lvert S_{11}\rvert$ bandwidth (%)	3 dB AR bandwidth (%)	HPBWs (°)	Max gain (dBic)	Radiation efficiency (%)
Proposed antenna	$0.211\lambda_0 \times 0.211\lambda_0 \times 0.057\lambda_0$	5.5 6.1	4.2 2.6	120 116	3.4 2.9	77 72
Ref. [5]	$0.23\lambda_0 \times 0.23\lambda_0 \times 0.07\lambda_0$	≥20 ≥20	Exact values not specified	≤100 ≤100	3.6 3.8	86 82
Ref. [6]	$0.47\lambda_0 \times 0.42\lambda_0 \times 0.098\lambda_0$	12.7 11.4	1.9 2.1	≤80 ≤80	5.0 7.0	Exact values not specified
Ref. [13]	$0.448\lambda_0 \times 0.448\lambda_0 \times 0.077\lambda_0$	2.3 7.2	0.6 1.4	≤80 ≤80	4.3 6.4	Exact values not specified
Ref. [14]	$0.491\lambda_0 \times 0.491\lambda_0 \times 0.164\lambda_0$	6.3 22.0	1.9 7.3	≤80 ≤80	6.3 7.5	90 97.4
Ref. [16]	$0.368\lambda_0 \times 0.368\lambda_0 \times 0.122\lambda_0$	1.4 6.5	0.8 2.2	82 82	7.0 6.7	95 87
Ref. [17]	$0.483\lambda_0 \times 0.483\lambda_0 \times 0.015\lambda_0$	2.3 3.0	0.6 0.7	100 114	3.9 3.9	Exact values not specified
Ref. [21]	$0.52\lambda_0 \times 0.52\lambda_0 \times 0.224\lambda_0$	≥10 ≥10	≥10 ≥10	135 112	4.2 4.2	Exact values not specified

from Figure 9(a), with L_{i1} varying from 7 nH to 9 nH, that the resonant frequencies at both bands decrease. The same phenomenon can be found in Figure 9(b) with L_{i2} varying from 1 nH to 1.4 nH at the high band. But with the increment of L_{i2}, the resonant frequency at the low band changes slightly. It means that by increasing the inductance of the inserted chip inductors, the effective electrical length of the antenna increases; thus, the compactness can be obtained.

4. Simulated and Measured Results

The ANSYS High-Frequency Structure Simulator (HFSS) is used to investigate and optimize the antenna configuration. A prototype of the proposed antenna is fabricated and measured as shown in Figure 10. The $\lvert S_{11}\rvert$ is measured with the Wiltron 37269A vector network analyzer, and the radiation patterns and ARs are measured in an anechoic chamber.

The simulated and measured $\lvert S_{11}\rvert$ is plotted in Figure 11, and a good agreement can been seen between the simulated and measured results. The measured impedance bands ($\lvert S_{11}\rvert < -10$ dB) range from 1.236 to 1.308 GHz and from 1.52 to 1.616 GHz, with the relative bandwidths of 5.5% and 6.1%. The simulated and measured ARs at the boresight direction are plotted in Figure 12. The measured AR bands (AR < 3 dB) are 54 MHz (1.232–1.286 GHz) and 40 MHz (1.532–1.572 GHz), with the relative bandwidths of 4.2% and 2.6%.

The simulated and measured radiation patterns at 1.268 GHz and 1.561 GHz are plotted in Figure 13. At 1.268 GHz, the proposed antenna yields wide HPBWs of 120° and 125° in the XOZ and YOZ planes, while the measured 3 dB AR beamwidths are 116° and 120° in the XOZ and YOZ planes, respectively, as shown in Figure 14(a). At 1.561 GHz, the proposed antenna yields HPBWs of 121° and 116° in the XOZ and YOZ planes, while the measured 3 dB AR beamwidths are 119° and 115°, respectively, as shown in Figure 14(b). The measured antenna gains at the boresight direction for 1.268 GHz and 1.561 GHz are 3.4 and 2.9 dBic, while the measured antenna radiation efficiencies can reach up to 77% and 72% as shown in Figure 15, respectively. The radiation efficiencies of the antenna are slightly lower than those of the antennas in the references due to the compactness and the inserted chip inductors. Discrepancies between measured and simulated results are likely due to substrate and measurement errors.

Table 1 shows the comparison of the measured performance of the proposed antenna with those of previous dual-band GNSS antennas. As shown in Table 1, the proposed antenna shows a compact dimension with wider HPBWs at both bands compared with other antennas.

5. Conclusion

A compact dual-band CP antenna with wide HPBWs for CNSS applications has been proposed and experimentally demonstrated in this paper by adopting the shorting loaded technique and inserting chip inductors. Four compact inverted-F monopoles are arranged symmetrically to the center point and fed by a compact SP feeding network. The proposed antenna exhibits two overlapped impedance and AR bandwidths of 50 MHz (1.236–1.286 GHz) and 40 MHz (1.532–1.572 GHz), covering the CNSS-2 B3 and B1 bands. Meanwhile, the HPBWs at 1.268 GHz and 1.561 GHz are both greater than 115° with a compact dimension of $0.211\lambda_0 \times 0.211\lambda_0 \times 0.057\lambda_0$. With these advantages, the antenna can be widely used in CNSS applications.

Conflicts of Interest

The authors declare that they have no conflicts of interest.

References

[1] J. Long and D. F. Sievenpiper, "A compact broadband dual-polarized patch antenna for satellite communication/navigation applications," *IEEE Antennas and Wireless Propagation Letters*, vol. 14, pp. 273–276, 2015.

[2] M. Chen and C.-C. Chen, "A compact dual-band GPS antenna design," *IEEE Antennas and Wireless Propagation Letters*, vol. 12, pp. 245–248, 2013.

[3] S. Gupta and G. Mumcu, "Dual-band miniature coupled double loop GPS antenna loaded with lumped capacitors and inductive pins," *IEEE Transactions on Antennas and Propagation*, vol. 61, no. 6, pp. 2904–2910, 2013.

[4] Nasimuddin, X. Qing, and Z. N. Chen, "A compact circularly polarized slotted patch antenna for GNSS applications," *IEEE Transactions on Antennas and Propagation*, vol. 62, no. 12, pp. 6506–6509, 2014.

[5] C. Sun, H. Zheng, and Y. Liu, "Compact dual-band circularly polarised GNSS antenna," *Electronics Letters*, vol. 51, no. 20, pp. 1559-1560, 2015.

[6] T. N. Chang and J. M. Lin, "Corner-fed dual-band circularly polarised antenna," *IET Microwaves, Antennas & Propagation*, vol. 8, no. 15, pp. 1423–1431, 2014.

[7] K. Agarwal, Nasimuddin, and A. Alphones, "Triple-band compact circularly polarised stacked microstrip antenna over reactive impedance meta-surface for GPS applications," *IET Microwaves, Antennas & Propagation*, vol. 8, no. 13, pp. 1057–1065, 2014.

[8] K. Agarwal and S. Dutta, "Miniaturized circularly polarized stacked patch antenna on reactive impedance surface for dual-band ISM and WiMAX applications," *International Journal of Antennas and Propagation*, vol. 2015, Article ID 938565, 10 pages, 2015.

[9] K. Zhang, C. Liu, X. Liu, H. Guo, and X. Yang, "Miniaturized circularly polarized implantable antenna for ISM-band biomedical devices," *International Journal of Antennas and Propagation*, vol. 2017, Article ID 9750257, 9 pages, 2017.

[10] Y. Li, S. Sun, and F. Yang, "A miniaturized Yagi-Uda-oriented double-ring antenna with circular polarization and directional pattern," *IEEE Antennas and Wireless Propagation Letters*, vol. 12, pp. 945–948, 2013.

[11] M. Ramirez, J. Parron, J. M. Gonzalez-Arbesu, and J. Gemio, "Concentric annular-ring microstrip antenna with circular polarization," *IEEE Antennas and Wireless Propagation Letters*, vol. 10, pp. 517–519, 2011.

[12] Y. Li, B. Tian, J. Xue, and G. Ge, "Compact dual-band circularly polarized antenna design for navigation terminals," *IEEE Antennas and Wireless Propagation Letters*, vol. 15, pp. 802–805, 2016.

[13] K. Chen, J. Yuan, and X. Luo, "Compact dual-band dual circularly polarised annular-ring patch antenna for BeiDou Navigation Satellite System application," *IET Microwaves, Antennas & Propagation*, vol. 11, no. 8, pp. 1079–1085, 2017.

[14] S. X. Ta, I. Park, and R. W. Ziolkowski, "Dual-band wide-beam crossed asymmetric dipole antenna for GPS applications," *Electronics Letters*, vol. 48, no. 25, pp. 1580-1581, 2012.

[15] K. Saurav, D. Sarkar, and K. V. Srivastava, "Dual-band circularly polarized cavity-backed crossed-dipole antennas," *IEEE Antennas and Wireless Propagation Letters*, vol. 14, pp. 52–55, 2015.

[16] S. X. Ta and I. Park, "Dual-band operation of a circularly polarized four-arm curl antenna with asymmetric arm length," *International Journal of Antennas and Propagation*, vol. 2016, Article ID 3531089, 10 pages, 2016.

[17] X. L. Bao and M. J. Ammann, "Dual-frequency dual circularly-polarised patch antenna with wide beamwidth," *Electronics Letters*, vol. 44, no. 21, pp. 1233-1234, 2008.

[18] Z. N. Chen, W. K. Toh, and X. Qing, "A microstrip patch antenna with broadened beamwidth," *Microwave and Optical Technology Letters*, vol. 50, no. 7, pp. 1885–1888, 2008.

[19] W. Q. Cao, B. N. Zhang, A. J. Liu et al., "A low-profile CP microstrip antenna with broad beamwidth based on loading with curved microstrip resonant structures," *Journal of Electromagnetic Waves and Applications*, vol. 26, no. 11-12, pp. 1602–1610, 2012.

[20] Y. X. Sun, K. W. Leung, and K. Lu, "Broadbeam cross-dipole antenna for GPS applications," *IEEE Transactions on Antennas and Propagation*, vol. 65, no. 10, pp. 5605–5610, 2017.

[21] S. L. Zuo, L. Yang, and Z. Y. Zhang, "Dual-band CP antenna with a dual-ring cavity for enhanced beamwidth," *IEEE Antennas and Wireless Propagation Letters*, vol. 14, pp. 867–870, 2015.

[22] C.-W. Su, S.-K. Huang, and C.-H. Lee, "CP microstrip antenna with wide beamwidth for GPS band application," *Electronics Letters*, vol. 43, no. 20, pp. 1062-1063, 2007.

[23] X. Ye, M. He, P. Zhou, and H. Sun, "A compact single-feed circularly polarized microstrip antenna with symmetric and wide-beamwidth radiation pattern," *International Journal of Antennas and Propagation*, vol. 2013, Article ID 106516, 7 pages, 2013.

[24] S. He and J. Deng, "Compact and single-feed circularly polarised microstrip antenna with wide beamwidth and axial-ratio beamwidth," *Electronics Letters*, vol. 53, no. 15, pp. 1013–1015, 2017.

[25] S. X. Ta and I. Park, "Compact wideband sequential-phase feed for sequentially rotated antenna arrays," *IEEE Antennas and Wireless Propagation Letters*, vol. 16, pp. 661–664, 2017.